

Robot Sound Interpretation: Combining Sight and Sound in Learning-Based Control

Peixin Chang, Shuijing Liu, Haonan Chen, and Katherine Driggs-Campbell

Abstract—We explore the interpretation of sound for robot decision-making, inspired by human speech comprehension. While previous methods use natural language processing to translate sound to text, we propose an end-to-end deep neural network which directly learns control policies from images and sound signals. The network is trained using reinforcement learning with auxiliary losses on the sight and sound network branches. We demonstrate our approach on two robots, a TurtleBot3 and a Kuka-IIWA arm, which hear a command word, identify the associated target object, and perform precise control to reach the target. For both systems, we perform ablation studies in simulation to show the effectiveness of our network empirically. We also successfully transfer the policy learned in simulator to a real-world TurtleBot3, which effectively understands word commands, searches for the object, and moves toward that location with more intuitive motion than a traditional motion planner with perfect information.

I. INTRODUCTION

People interpret sounds they hear and interact with the world according to their interpretations. Every speech sound signal contains more than just the associated word—there is intent and sentiment that we learn to intuit. When a human maps sound to meaning, the brain forms conceptual representations of words [1]. Inspired by humans’ natural speech comprehension, we explore whether the sound command can be directly interpreted by the robots for visual-based decision making rather than being transcribed into text and symbols. By integrating sound and sight with decision-making and control, we begin to enable collaborative robots that seamlessly integrate with people in everyday life.

Consider the scenarios in Figure 1. Given a sound command, the robot must identify the corresponding target from the set of objects. To achieve this goal, the robots have to draw the correspondence between the visual and audio inputs, and learn a policy to reach the target. The temporally related sound data and the vast diversity of word utterances poses challenges for recognition and in turn decision-making based on the sound inputs. We propose an end-to-end framework which uses model-free deep Reinforcement Learning (RL) for decision-making and Recurrent Neural Networks (RNNs) with attention mechanisms for sound signal processing. Our network combines representations from the physical state, vision, and sound, thus enabling robots to relate information from multiple modalities.

P. Chang, S. Liu, and K. Driggs-Campbell are with the Department of Electrical and Computer Engineering at the University of Illinois at Urbana-Champaign. emails: {pchang17,slui105,krdc}@illinois.edu

H. Chen is with the Computer Engineering Department at Zhejiang University-University of Illinois at Urbana-Champaign Institute. email: haonan2@illinois.edu

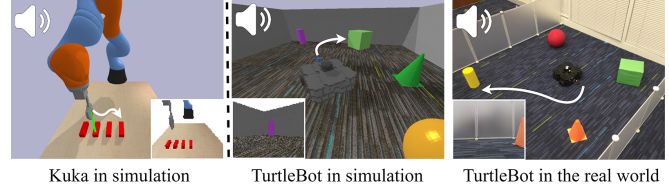


Fig. 1: **Illustration of our robotic environments.** Windowed image shows the robot camera view. *Left:* The Kuka moves its gripper tip to the target block chosen from four identical blocks. *Middle:* TurtleBot searches for, then navigates to the target object among four objects. *Right:* Experimental setup showing transfer of learned policy to a real-world system.

There has been a great deal of research effort in integrating voice in robotics. Motivated by human’s spoken language communication, many robotics researchers have investigated voice controlled robots. The usual pipeline consists of three stages. First, the speech signal is processed by an automatic speech recognition (ASR) system, which transforms speech to text [2], [3], [4]. Second, the text is processed by a language model, which links the text to the logic relations or entities in the physical world [5]. Third, the robot performs actions based on the analysis from the second stage [6], [7], [8], [9], [10]. This pipeline applies to large corpuses and can handle sentence (or even multiple sentences) inputs.

Robots designed with this pipeline rely on predefined representation of sounds in the form of texts and symbols, while our model actively learns and builds its own numerical interpretation of sounds, which we call *Robot Sound Interpretation*. In contrast to the predefined representation, the learned interpretation can change and evolve dynamically when a robot interacts with the environment, which is similar to that of a human. The preprocessing of sound can also be remarkably simplified, because the sound feature representations are used directly for communication without being translated into another media for manipulation. In addition, voice controlled robots tend to neglect the rich information stored in some non-speech signals, while our model accepts both speech and non-speech signals.

Cognitive architectures such as [11], [12] also attempt to mimic the process of human speech comprehension. However, the architectures in these works directly map sounds to predefined robot actions in an one-to-one manner, making the agents less capable of performing long-term decision making [11]. Further, these works typically only utilize the sound modality, overlooking the interplay between sound and sight [13]. Our model actively learns a complex action sequence combining information from images and audios.

Inspired by the recent success of deep learning, situated language learning agents have been developed to execute

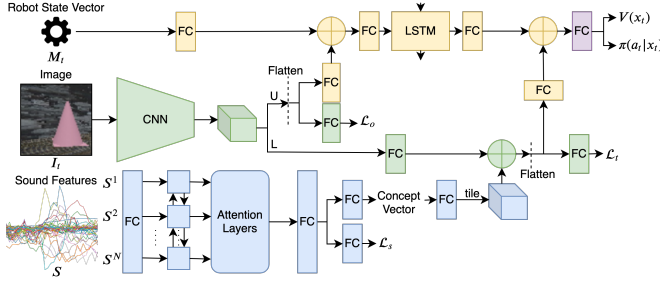


Fig. 2: **The network architecture.** The sound encoder is in blue, the visual-motor integrator is in yellow and green, and the policy learner is in purple. The losses \mathcal{L}_o and \mathcal{L}_t are only needed in the more challenging TurtleBot environment, while \mathcal{L}_s is applied in both environments. We use \oplus to denote element-wise addition and FC to denote fully connected layers.

tasks such as navigation [14], [15], [16] and object finding [17], [18] according to natural language instructions and images. These works successfully show that a robot may learn to understand language and grounding in an end-to-end fashion. These studies, however, are typically conducted in highly controlled and simulated environments with simple action models, and none of these learning agents have been transferred to a physical robot platform for performing a real-world task. Moreover, these agents take text-based instructions, not sound signals, and thus abstracting away the complexities of speech and limiting the potential of human-robot communication. In contrast, we use raw acoustic signals as one of the multi-modal inputs to the system and demonstrate our robot task in simulation and the real-world.

We present the following contributions: (1) We present the novel concept of Robot Sound Interpretation—learning policies directly from sound commands without translating sound to text. (2) We develop a network architecture that is trained end-to-end without hand-crafted features, allowing us to use a wide variety of sound inputs on different robot environments. (3) Our network exhibits promising results in two robot platforms: a Kuka-IIWA and TurtleBot3 in simulation. The TurtleBot3 policy was successfully transferred to a real-world TurtleBot3 without training on real-world data.

This paper is organized as follows: In Section II, we formalize the problem and propose our network architecture. Experiments in simulation and in the real-world are discussed in Section III and Section IV, respectively. Finally, we conclude the paper in Section V.

II. METHODOLOGY

A. Problem formulation

Consider an agent interacting with an episodic environment \mathcal{E} . We model this interaction as a Markov Decision Processes, defined by the tuple $\langle \mathcal{X}, \mathcal{A}, P, R, \gamma, \mathcal{X}_0 \rangle$. For each episode, the agent begins at a randomly selected initial state $x_0 \in \mathcal{X}_0$. At each time step t , the state $x_t = \{S, I_t, M_t\} \in \mathcal{X}$ of the agent consists of three parts: an one-time sound feature (S) representing the command, an image (I_t) from its camera, and a robot state vector (M_t) which includes information such as manipulators' end effector location or locomotors' odometry. The agent then takes an action $a_t \in \mathcal{A}$ according to its policy $\pi_\theta(a_t|x_t)$ parameterized by θ . In

return, the agent receives a reward r_t and transits to the next state x_{t+1} according to an unknown state transition $P(\cdot|x_t, a_t)$. The process continues until t exceeds the maximum episode length T and the next episode starts. The goal of the agent is to maximize the discounted sum of future return $R_t = \sum_{i=t}^{\infty} \gamma^{i-t} r_i$. The value of state x under policy π is defined as $V^\pi(x) = \mathbb{E}[R_t|x_t = x]$ and is the expected return for following policy π from state x .

B. Network Architecture

The proposed network, as shown in Figure 2, is comprised of three major sub-modules: the sound encoder, the visual-motor integrator, and the policy learner.

1) *The sound encoder:* The sound encoder takes in sound feature S and outputs an encoding, which we call the concept vector C . This vector encapsulates the information for the sound and mimics the functionality of humans' conceptual representations of words when they map sound to meaning. This vector is the agent's own interpretation of the sound, which is formed through its interaction with the environment. The sound feature $S \in \mathbb{R}^{N \times m}$ is the Mel Frequency Cepstral Coefficients (MFCCs) of the raw acoustic signal [19], where N is the number of frames of the signal and the m is the number of MFCCs for a frame. We use S^j to denote the j^{th} frame of S , where $j \in \{1, 2, \dots, N\}$.

A single layer bi-directional long short-term memory (BiLSTM) network with number of units d_S and zero initial state is used to encode S [20]. Let $h_j = [\vec{h}_j^\top, \overleftarrow{h}_j^\top]^\top \in \mathbb{R}^{2d_S}$ be the concatenated output of the forward and backward cells of the BiLSTM at frame j . The BiLSTM output for S is $h = [h_1^\top; h_2^\top; \dots; h_N^\top] \in \mathbb{R}^{N \times 2d_S}$. An attention layer over the BiLSTM is applied to select the relevant temporal locations over the input sequence. The final hidden states h_N is first expanded to a $N \times 2d_S$ matrix. Let $h_A \in \mathbb{R}^{N \times 4d_S}$ be the result of concatenation between h and the expanded h_N . The unnormalized score $e \in \mathbb{R}^N$ for h is $e = f(h_A)v_A$, where $f(\cdot)$ are fully connected layers, the last of which has l units, and $v_A \in \mathbb{R}^l$ are trainable weights. The weight $\alpha \in \mathbb{R}^N$ for each h_j in h is calculated by a softmax function: $\alpha = \text{softmax}(e)$. The weighted sum of these h_j , denoted $c \in \mathbb{R}^{2d_S}$, is computed by multiplying the concatenated output of the BiLSTM with the weight $\alpha \in \mathbb{R}^N$: $c = h^\top \alpha$. The concept vector is given by $C = g(c)$, where $g(\cdot)$ are fully connected layers with tanh activation that transforms c into a 64-dimensional vector.

Compared to the attention mechanism used in the literature of neural machine translation and automatic speech recognition [21], [22], [23], our attention mechanism uses a score function that does not depend on a decoder state, as our model does not explicitly have a decoder. We found multi-head attention beneficial in our tasks [24]. In multi-head attention, each head generates a different attention distribution, which allows the model to learn to attend to different locations. The agent using multi-head attention usually achieves a slightly higher average reward.

The sound encoder only encodes S at the first time step. The resulting C is cached and shared throughout the episode,

which captures the fact that the sound is transient, while the concept persists. We add an auxiliary adaptation loss \mathcal{L}_s in the sound encoder, which predicts the label of the received acoustic signal. The \mathcal{L}_s is a multi-class classification loss which helps the sound encoder for feature extractions.

2) *Visual-motor integrator*: The visual-motor integrator takes the concept vector C produced by the sound encoder, the current visual observation I_t , and the current robot state vector M_t as the inputs and creates a joint representation which will be used by the policy learner. The image I_t is processed by a VGG-style convolution neural network (CNN) [25], the output of which is shared by two branches denoted by U and L in Fig. 2. The upper branch U merges with the features extracted from the robot state vector, and the resulted vector is fed into a single-layer LSTM, whose output is responsible for agent’s visual-motor skill. The LSTM allows the model to capture information from the past, which is important for a partially observable environment. The lower branch L merges with the information from the concept vector C , which forms a joint representation between images and the agent’s interpretation of the sound.

The visual-motor integrator includes two task specific auxiliary losses, \mathcal{L}_o and \mathcal{L}_t . The loss \mathcal{L}_o is a multi-label classification loss that predicts which of the four objects are in I_t , providing a guidance of visual feature extraction for object recognition. The loss \mathcal{L}_t is a binary classification loss that predicts whether the target object is in I_t , and thus builds an association between the command heard by the agent and the corresponding object in the arena.

3) *Policy learner*: The output of the visual-motor integrator is fed into the policy learner, whose loss function is denoted as \mathcal{L}_{pg} . We use Proximal Policy Optimization (PPO), a model-free policy gradient algorithm, for policy and value function learning [26]. We adopt the implementation from OpenAI Baselines and modify the original implementation so as to incorporate various types of observation from the environment [27]. Eight instances of the environment run in parallel for collecting the agent’s experiences, which both accelerates and stabilizes learning. When updating the policy, the entire history of four episodes is used for an update.

Our loss function \mathcal{L}_{tot} is a linear combination of \mathcal{L}_{pg} , \mathcal{L}_s , \mathcal{L}_o , and \mathcal{L}_t , giving:

$$\mathcal{L}_{tot} = w_{pg}\mathcal{L}_{pg} + w_s\mathcal{L}_s + w_o\mathcal{L}_o + w_t\mathcal{L}_t \quad (1)$$

where w_{pg} , w_s , w_o , and w_t are the scalar weights for each loss. We set $w_{pg} = w_s = 1$ for both environments, $w_o = w_t = 0$ for the Kuka environment, and $w_o = w_t = 0.5$ for the TurtleBot environment. The learning rate is $8e^{-6}$.

III. SIMULATION EXPERIMENTS

In this section, we describe the sound data processing and present two test cases in two robotic environments, as well as training and testing the models in simulation.

A. Sound data processing

We consider two types of sound signals in our model: single-word speech signals and single-tone non-speech signals. For speech signals, we use the Speech Commands

Dataset, which contains 65,000 one-second long utterances of 30 short words collected from thousands of different people [28]. Two sets of words are chosen from these 30 words for the experiments. Wordset1 contains the utterances of four numbers: “zero,” “one,” “two,” and “three.” Wordset2 includes the utterances of four object names: “house,” “tree,” “bird,” and “dog.” In the data preprocessing stage, we clean the dataset by removing highly distorted and blank recordings. For each word in the two sets, 1,000 samples are used for training and 50 samples are used for testing.

For non-speech signals, we use NSynth dataset, an audio dataset containing 305,979 musical notes, each with a unique pitch, timbre, and envelope [29]. The musical notes we use are C_4 (Middle C), D_4 , E_4 , and F_4 . The musical instruments for performing those notes include guitar, keyboard, and string. For each of the four musical notes, 1,000 samples are used for training and 50 samples are used for testing.

When extracting the MFCCs for the sound signal, we use 40 filters in the filter bank and 40 coefficients [30]. The resulted MFCCs is padded with zeros if the number of frames is less than 100 so that the sound feature $S \in \mathbb{R}^{100 \times 40}$.

B. Robotic Environments

We examine different robot platforms as well as fully and partially observable environments. We design two environments which are implemented in PyBullet [31]. The Kuka environment uses a location-fixed Kuka-IIWA arm, while the TurtleBot environment uses a mobile TurtleBot3 Waffle Pi.

1) *TurtleBot*: The TurtleBot environment consists of a $2m \times 2m$ arena and four fix-sized 3D objects: a cube, a sphere, a cone, and a cylinder. The action $a = [\delta_v, \delta_a]^T$, where δ_v is the increment of the desired transitional velocity v_d in m/s , and δ_a is the increment of the desired angle ϕ_d in rad with respect to robot’s initial orientation. We define the update rule for v_d and ϕ_d with respect to time t as

$$\begin{aligned} v_d[t] &= 0.05\delta_v + v_d[t-1] \\ \phi_d[t] &= 0.15\delta_a + \phi_d[t-1] \end{aligned} \quad (2)$$

We apply a simple proportional control on the desired angle. The proportional gain is 1.5.

We match each object with one word or note. When an episode begins, the robot is placed randomly near the center of the arena. The four objects with randomly chosen color are placed randomly around the robot. The environment then randomly chooses one sound from one of the four words or musical notes. The MFCCs of the sound, S , are extracted. At every timestep, the TurtleBot receives a $75 \times 100 \times 3$ RGB image from its camera, which is cropped and resized to I_t of size $96 \times 96 \times 3$ for CNN processing. The robot state vector $M_t = [v_d[t], \phi_d[t]]$. The time horizon, T , is 80. We define the reward $r_t = r_c + r_{dis} + r_a + r_{goal}$. Let d_t and β_t be the safe distance and angle from the camera’s central axis to the target object at time t . The collision penalty, r_c , is -0.1 if the robot is too close to the target object and -0.3 if the robot is too close to the other objects and the wall.

$$\begin{aligned} r_{dis} &= 50(-|d_t| + |d_{t-1}|) \\ r_a &= 20(-|\beta_t| + |\beta_{t-1}|) \end{aligned} \quad (3)$$

$$r_{goal} = \begin{cases} 2, & \text{if } z_d^- \leq d_t \leq z_d^+ \text{ and } z_\beta^- \leq |\beta_t| \leq z_\beta^+ \\ 0.5, & \text{if } z_d^- \leq d_t \leq z_d^+ \text{ or } z_\beta^- \leq |\beta_t| \leq z_\beta^+ \\ 0, & \text{otherwise.} \end{cases}$$

where z_d^+ and z_d^- are the upper and lower limits on the goal distance, and z_β^+ and z_β^- are the upper and lower limits on the goal angle. Intuitively, the agent gets high reward when it approaches to the target, while maintaining a safe distance.

2) *Kuka*: The Kuka environment consists of a table, a Kuka-IIWA arm, and four identical blocks with length 0.1m and width 0.04m. The blocks are placed in a line parallel to one side of the table in front of the robot, and the space between two neighboring blocks is fixed as 0.06m. The gripper tip can only move within an xy-plane, above the table top. The action $a = [\delta_x, \delta_y]^\top$, where δ_x is the increment of the desired gripper tip location in the x axis p_x , and δ_y is the increment of that in y axis p_y at time t . We define the update rule for p_x and p_y with respect to time t as

$$\begin{aligned} p_x[t] &= 0.01\delta_x + p_x[t-1] \\ p_y[t] &= 0.01\delta_y + p_y[t-1] \end{aligned} \quad (4)$$

Both p_x and p_y will be clipped to be within a certain range to limit the space where the gripper tip can move and are used for calculating the inverse kinematics of the arm. We use position control for controlling the joints of the robot.

We match each block with one word or note. When an episode begins, the location of the gripper tip and the blocks are initialized randomly, and the environment randomly chooses one sound from one of the four words. The MFCCs of the sound, S , are extracted. At every timestep, the agent receives an $80 \times 80 \times 1$ black and white image I_t from a RGB camera fixed at a location. From the image, the robot can always see the four blocks and its gripper tip. The robot state vector $M_t = [l_x[t], l_y[t]]^\top$, where $l_x[t]$ and $l_y[t]$ are the gripper tip location at time t . The time horizon T is 200. We define the reward $r_t = r_{dis} + r_{goal}$. Let d_t be the distance between the robot gripper tip and the target block center at time t in the xy-plane, then r_{dis} and r_{goal} is defined as

$$\begin{aligned} r_{dis} &= -0.5d_t - 0.1(\ln(d_t^2 + 5 \times 10^{-5}) + 3.5), \\ r_{goal} &= \begin{cases} 1, & \text{if } M_t \in A \\ 0, & \text{otherwise.} \end{cases} \end{aligned} \quad (5)$$

where A is the area right above the target block. Intuitively, the agent gets high reward when its gripper is at the center of the target block.

Agents trained in these environments will encounter different difficulties. The agent in the Kuka environment needs to develop spatial reasoning skills that can differentiate the target object from the four identical blocks using their relative positional information observed from only one camera. The agent in the TurtleBot environment needs to learn exploration skills so as to find the target object as quickly as possible.

C. Experiment setup

We now introduce the training procedure and evaluation of our network in simulation. In our experiments, the overall

architecture of the network is kept the same in both TurtleBot and Kuka environments, except the following modifications.

In TurtleBot environment, we pretrain the vision module (green component in Fig. 2) to accelerate the convergence of the whole network. We collect image data through an automatic process for all sixteen labels in simulator to optimize \mathcal{L}_o , where each label indicates whether an object is in I_t . Using the label of these image, we optimize \mathcal{L}_t by replacing the concept vector to randomly generated one-hot vectors. TurtleBot environment requires a deeper CNN and a deeper LSTM to achieve good performance, because the partial observability of this environment adds complexity to the robot's task. We train the network for 1.5×10^6 timesteps.

In Kuka environment, we train our network without pre-trained weights as the task requires less exploration to obtain a good policy. \mathcal{L}_o and \mathcal{L}_t are no longer needed since all four identical blocks are always in the robot's fixed camera view. We train the network for 5×10^6 timesteps.

1) *Evaluation criteria*: In simulation, we test the policy for 200 episodes (50 for each target object) with unheard sound data. For TurtleBot environment, we define an episode as success if the distance between the robot and the target object is no more than 0.34m. For Kuka environment, we define an episode as success if the distance between the gripper tip and the center of target block is below 0.04m. We define success rate as the percentage of successful episodes in all test episodes and use it as our metric.

2) *Baselines*: We introduce an oracle with perfect sound concept vector and a random walk baseline as good and poor standards for comparison. To examine the limits of our network's performance, we train an oracle model by replacing the concept vector with an one-hot vector corresponding to the target object. Thus, the sound encoder of the oracle is 100% accurate, which should allow the oracle to exhibit close-to-optimal performance for a traditional RL agent. For all other models, the closer the model's performance gets to the oracle's, the better it is. For the random walk baseline, the robots take a random action at each timestep without any training. The performance of a model is reasonable if it has higher success rates than the baseline.

D. Results

The following subsections outline our quantitative and qualitative assessment of the system performance. We examine the learning ability, task performance, and sensitivity of our proposed system. For quantitative measures, we conduct a thorough ablation study on the auxiliary losses used, the attention mechanism designed to guide the sound encoder, and the sensitivity of the sounds used to command the robot.

1) *Auxiliary losses*: We analyze the performance of models with auxiliary losses ablated, from both training and testing perspective.¹ We find that \mathcal{L}_s (gray in Fig. 3), helps feature extraction for the sound encoder. For the Kuka task, the model with \mathcal{L}_s can achieve 10% higher success rate at the test time (Table I), meaning that the agent learns more robust

¹The results of Wordset1, Wordset2, and NSynth are similar in ablations of auxiliary losses, so we take Wordset1 as an example to analyze.

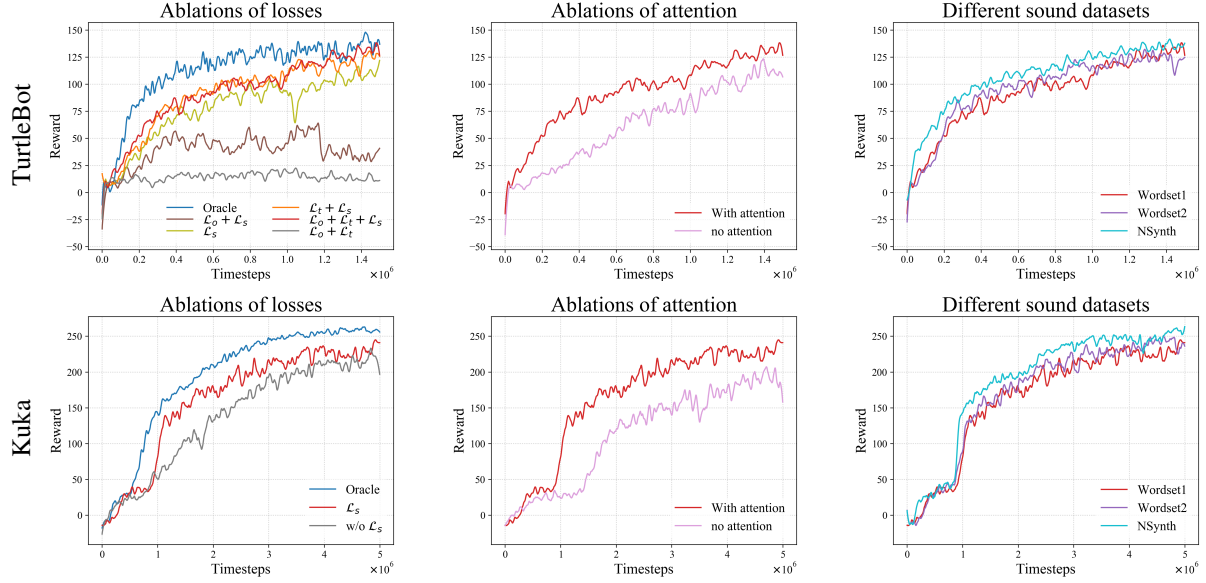


Fig. 3: **Training curves of our network in TurtleBot environment (top) and Kuka environment (bottom).** *Left:* Comparison of our trained model with the oracle and models without different kinds of auxiliary losses. All models have 4 attention heads and are trained with Wordset1. *Middle:* Comparison of our model with and without attention mechanism, both of which have all three auxiliary losses and are trained with Wordset1. *Right:* Comparison of our model trained with different sound data, all of which have all three auxiliary losses and 4 attention heads.

features from \mathcal{L}_s . For the more complex TurtleBot environment, the \mathcal{L}_s provides a guidance for sound interpretation, which eases the process of policy search.

For the TurtleBot task, removing $\mathcal{L}_t + \mathcal{L}_o$ (olive) or \mathcal{L}_o (orange) in Fig. 3 left, does not significantly affect training. The loss’s impact is partially handled by the pretrained weights, which also minimize $\mathcal{L}_t + \mathcal{L}_o$. However, the success rate is reduced for $\sim 9\%$ in testing (Table I). We believe there are two reasons for this: (1) When the robot encounters new situations unseen by the pretraining data, it cannot draw guidance from \mathcal{L}_o . (2) The concept vector from real sound data is distinctive from the one-hot vector used in pretraining. The agent cannot rebuild the association between the command heard by the agent and the corresponding object in the arena using \mathcal{L}_t . Removing \mathcal{L}_t (brown) alone results in underfitting because the agent cannot differentiate which object is its target. Thus, the robot is biased towards reaching the first object insight to minimize \mathcal{L}_o . Therefore, optimizing all three auxiliary losses are essential for TurtleBot to achieve its goal.

2) *Attention vs. no attention:* To examine the effectiveness of the attention layer over the BiLSTM, we remove the attention layer from the network and train the network with all three sets of sound for both environments. The training curves in Fig. 3 (middle) shows that the removal of the attention layer negatively affects the training. Table II and Table III shows that for the two wordsets, models with attention exhibit 6%-15% higher performance than those without attention, which validates the necessity of attention layers. However, for NSynth dataset, attention layers do not make a difference because pure tone signals have simpler and cleaner patterns, which is easier for our network to learn.

3) *Robustness to sound type:* We use three sets of sound data in our experiments: Wordset1, Wordset2, and notes from

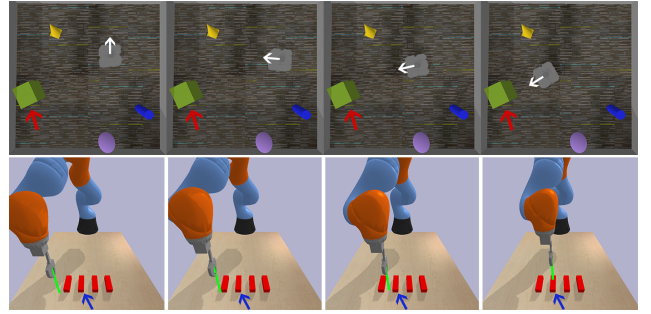


Fig. 4: **Trained model in simulation.** *Top:* Simulated TurtleBot searches and approaches its target, the green cube. The heading direction is shown by white arrows. *Bottom:* Kuka-IIWA correctly chooses the target block indicated by the blue arrow in simulator. The green vertical line indicates the location of the gripper tip on the table top. This line is invisible by the robot and is only for visualization purposes.

NSynth dataset. From the training curves (Fig. 3 (right)) and testing results (Table II and Table III), we found that the performance of models with distinct sound datasets exhibit very little difference in training and testing. This validates the robustness of our network with respect to the change of different types of sound sources.

4) *Qualitative simulation results:* In Fig. 4, the snapshots of the two robots in a test episode are shown. In most cases, after sufficient training, both robots are able to reach their respective goals well before an episode ends.

IV. REAL-WORLD EXPERIMENTS

We evaluate the performance of our trained model on a real TurtleBot3 Waffle Pi (Fig. 5). For this experiment, we assign “house” to the cube, “dog” to the sphere, “bird” to the cone, and “tree” to the cylinder.

To narrow the gap between rendered and real-world images, we use domain randomization to learn robust visual features [32]. We randomize the color and texture of the

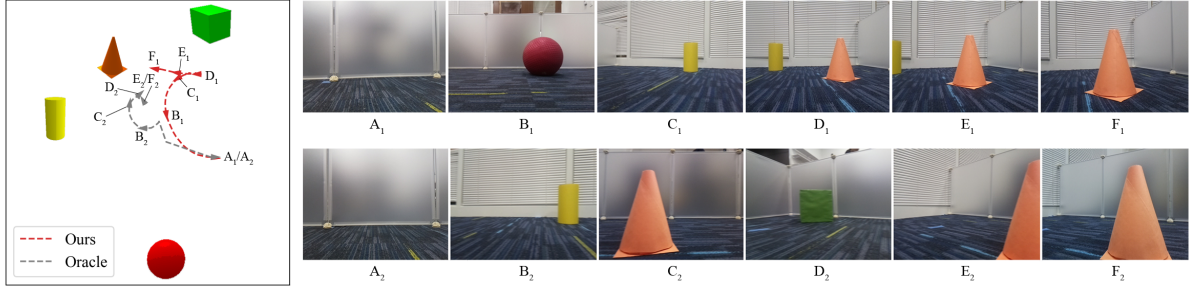


Fig. 5: **Policy execution of our model compared with human-controlled oracle in a real-world experiment.** The target is the cone. *Left*: Navigation map of TurtleBot controlled by our model (red) and human (gray). The arrows indicate the orientation of TurtleBot. *Right*: The same episode in TurtleBot's camera view. A_1 - F_1 and A_2 - F_2 are the checkpoints in two trajectories corresponding to the labels in the left subfigure.

TABLE I: Testing results of our model with ablations of auxiliary losses trained with Wordset1

Environment	Network	Success rate
TurtleBot	Attention+ $\mathcal{L}_o + \mathcal{L}_t + \mathcal{L}_s$	0.895
	Attention + $\mathcal{L}_o + \mathcal{L}_t$	0.135
	Attention + $\mathcal{L}_t + \mathcal{L}_s$	0.805
	Attention + $\mathcal{L}_o + \mathcal{L}_s$	0.350
	Attention + \mathcal{L}_s	0.790
	Attention	0.100
Kuka	Attention + \mathcal{L}_s	0.915
	Attention	0.805

TABLE II: Testing results of our model in TurtleBot environment with oracles, ablation of attention layer, and baselines

Sound Data	Network	Success rate
—	Oracle	0.975
Wordset1	Attention+ $\mathcal{L}_o + \mathcal{L}_t + \mathcal{L}_s$	0.895
	No attention + $\mathcal{L}_o + \mathcal{L}_t + \mathcal{L}_s$	0.800
Wordset2	Attention + $\mathcal{L}_o + \mathcal{L}_t + \mathcal{L}_s$	0.870
	No attention + $\mathcal{L}_o + \mathcal{L}_t + \mathcal{L}_s$	0.735
NSynth	Attention + $\mathcal{L}_o + \mathcal{L}_t + \mathcal{L}_s$	0.920
	No attention + $\mathcal{L}_o + \mathcal{L}_t + \mathcal{L}_s$	0.930
—	Random walk	0.145

four objects, the arena wall, and the background using the textures from the Describable Textures Dataset during training [33]. Our model trained with domain randomization can be transferred to the real TurtleBot3 smoothly without further training on real world data.

In the real-world experiment, the communication between the TurtleBot3 and its host computer is established by the Robot Operating System (ROS) [34]. At every timestep, the trained agent receives an image captured by robot's RGB camera and the robot state vector calculated from odometry data and then produces an action. The wave files from the word datasets are used as the sound input. We run a total of 40 tests (10 for each word) and count the number of times the robot approaches the correct target object. The results of the experiment show that the success rates for each word are all 90.0%, which indicates that the simulation to real world transfer is successful, even though the size, shape, and texture of the objects in the real world are slightly different from these in the simulation. The agent fails usually when the target object is not recognized. In such cases, the agent still actively searches for the target object but fails at approaching.

To further evaluate the performance of our model in the

TABLE III: Testing results of our model in Kuka environment with oracles, ablations of attention layer, and baselines

Sound Data	Network	Success rate
—	Oracle	0.970
Wordset1	Attention + \mathcal{L}_s	0.915
	No attention+ \mathcal{L}_s	0.750
Wordset2	Attention + \mathcal{L}_s	0.910
	No attention+ \mathcal{L}_s	0.835
NSynth	Attention + \mathcal{L}_s	0.950
	No attention+ \mathcal{L}_s	0.945
—	Random walk	0.025

real world, we compare the policy of our model with that of an oracle which is controlled by a human. The human has the map of the whole arena, which is generated by the laser distance sensor on the TurtleBot3. After the human hears an utterance of a word, she drives the robot towards the target object by choosing the desired goal position and orientation of the TurtleBot3 on that map. The robot then moves to the goal by following the planner in the ROS `move_base` package [35]. We run five tests for each object. A typical example of the policy for our model and for the oracle is shown in Fig. 5. Our agent tends to find the target object with natural searching behavior. The robot usually first steps backward and rotates to look around for the target object. Once identified, it approaches towards the target until it is close to the object. The oracle favors a piecewise trajectory. Although less human-like, the direct trajectories usually have a shorter length compared to these of our model, owing to the fact that the oracle has the map of the arena. Nonetheless, this experiment shows that our model can achieve comparable result as a human controlled oracle.

V. CONCLUSION AND FUTURE WORK

We propose a novel end-to-end network for sound and vision-based robot control tasks. Our network integrates the image features from CNN, the sound features from a BiLSTM with attention, and the states of the robot to learn a policy using deep RL. We demonstrate our approach on TurtleBot and Kuka arm, and transferred the trained model to a real TurtleBot. Our experiments show promising results in both simulator and real world. Possible directions to explore in future work include: (1) generalizing the sound commands from single word to phrases and sentences, and (2) transferring our model to a Kuka-IIWA arm in real world.

REFERENCES

- [1] E. Kocagoncu, A. Clarke, B. J. Devereux, and L. K. Tyler, "Decoding the cortical dynamics of sound-meaning mapping," *Journal of Neuroscience*, vol. 37, no. 5, pp. 1312–1319, 2017.
- [2] F. Cruz, G. I. Parisi, J. Twiefel, and S. Wermter, "Multi-modal integration of dynamic audiovisual patterns for an interactive reinforcement learning scenario," in *IEEE/RSJ International Conference on Intelligent Robots and Systems (IROS)*, 2016, pp. 759–766.
- [3] R. A. S. Fernandez, J. L. Sanchez-Lopez, C. Sampedro, H. Bavlé, M. Molina, and P. Campoy, "Natural user interfaces for human-drone multi-modal interaction," in *IEEE International Conference on Unmanned Aircraft Systems (ICUAS)*, 2016, pp. 1013–1022.
- [4] B. Burger, I. Ferrané, F. Lerasle, and G. Infantes, "Two-handed gesture recognition and fusion with speech to command a robot," *Autonomous Robots*, vol. 32, no. 2, pp. 129–147, 2012.
- [5] E. Bastianelli, D. Croce, A. Vanzo, R. Basili, and D. Nardi, "A discriminative approach to grounded spoken language understanding in interactive robotics," in *International Joint Conference on Artificial Intelligence (IJCAI)*, 2016, pp. 2747–2753.
- [6] F. Stramandinoli, V. Tikhonoff, U. Pattacini, and F. Nori, "Grounding speech utterances in robotics affordances: An embodied statistical language model," in *Joint IEEE International Conference on Development and Learning and Epigenetic Robotics (ICDL-EpiRob)*, 2016, pp. 79–86.
- [7] R. Paul, J. Arkin, D. Aksaray, N. Roy, and T. M. Howard, "Efficient grounding of abstract spatial concepts for natural language interaction with robot platforms," *The International Journal of Robotics Research*, vol. 37, no. 10, pp. 1269–1299, 2018.
- [8] R. Liu, J. Webb, and X. Zhang, "Natural-Language-Instructed Industrial Task Execution," in *International Design Engineering Technical Conferences and Computers and Information in Engineering Conference*, vol. Volume 1B: 36th Computers and Information in Engineering Conference, 2016.
- [9] E. Ovchinnikova, M. Wachter, V. Wittenbeck, and T. Asfour, "Multi-purpose natural language understanding linked to sensorimotor experience in humanoid robots," in *IEEE-RAS 15th International Conference on Humanoid Robots (Humanoids)*, 2015, pp. 365–372.
- [10] R. Liu and X. Zhang, "A review of methodologies for natural-language-facilitated human-robot cooperation," *International Journal of Advanced Robotic Systems*, vol. 16, no. 3, 2019.
- [11] Y. Zhang and J. Weng, "Grounded auditory development by a developmental robot," in *International Joint Conference on Neural Networks (IJCNN)*, vol. 2, 2001, pp. 1059–1064.
- [12] Q. Liu, S. Levinson, Y. Wu, and T. Huang, "Robot speech learning via entropy guided ltv and memory association," in *International Joint Conference on Neural Networks (IJCNN)*, vol. 3, 2001, pp. 2176–2181.
- [13] P. Manoonpong, F. Pasemann, J. Fischer, and H. Roth, "Neural processing of auditory signals and modular neural control for sound tropism of walking machines," *International Journal of Advanced Robotic Systems*, vol. 2, no. 3, p. 22, 2005.
- [14] P. Anderson, Q. Wu, D. Teney, J. Bruce, M. Johnson, N. Sünderhauf, I. Reid, S. Gould, and A. van den Hengel, "Vision-and-language navigation: Interpreting visually-grounded navigation instructions in real environments," in *IEEE Computer Society Conference on Computer Vision and Pattern Recognition (CVPR)*, 2018, pp. 3674–3683.
- [15] H. Chen, A. Suhr, D. Misra, N. Snaveley, and Y. Artzi, "Touchdown: Natural language navigation and spatial reasoning in visual street environments," in *IEEE Computer Society Conference on Computer Vision and Pattern Recognition (CVPR)*, 2019, pp. 12 538–12 547.
- [16] H. Yu, H. Zhang, and W. Xu, "Interactive grounded language acquisition and generalization in a 2d world," in *International Conference on Learning Representations (ICLR)*, 2018.
- [17] K. M. Hermann, F. Hill, S. Green, F. Wang, R. Faulkner, H. Soyer, D. Szepesvari, W. M. Czarnecki, M. Jaderberg, D. Teplyaev, *et al.*, "Grounded language learning in a simulated 3d world," *arXiv preprint arXiv:1706.06551*, 2017.
- [18] D. S. Chaplot, K. M. Sathyendra, R. K. Pasumarthi, D. Rajagopal, and R. Salakhutdinov, "Gated-attention architectures for task-oriented language grounding," in *Thirty-Second AAAI Conference on Artificial Intelligence (AAAI)*, 2018, pp. 2819–2826.
- [19] S. Davis and P. Mermelstein, "Comparison of parametric representations for monosyllabic word recognition in continuously spoken sentences," *IEEE transactions on acoustics, speech, and signal processing*, vol. 28, no. 4, pp. 357–366, 1980.
- [20] M. Schuster and K. K. Paliwal, "Bidirectional recurrent neural networks," *IEEE Transactions on Signal Processing*, vol. 45, no. 11, pp. 2673–2681, 1997.
- [21] W. Chan, N. Jaitly, Q. V. Le, and O. Vinyals, "Listen, attend and spell," in *2016 IEEE International Conference on Acoustics, Speech and Signal Processing (ICASSP)*, 2016, pp. 4960–4964.
- [22] D. Bahdanau, K. Cho, and Y. Bengio, "Neural machine translation by jointly learning to align and translate," in *International Conference on Learning Representations (ICLR)*, 2015.
- [23] M.-T. Luong, H. Pham, and C. D. Manning, "Effective approaches to attention-based neural machine translation," in *Conference on Empirical Methods in Natural Language Processing (EMNLP)*, 2015, pp. 1412–1421.
- [24] A. Vaswani, N. Shazeer, N. Parmar, J. Uszkoreit, L. Jones, A. N. Gomez, L. Kaiser, and I. Polosukhin, "Attention is all you need," in *Advances in Neural Information Processing Systems (NIPS)*, 2017, pp. 5998–6008.
- [25] K. Simonyan and A. Zisserman, "Very deep convolutional networks for large-scale image recognition," in *International Conference on Learning Representations (ICLR)*, 2015.
- [26] J. Schulman, F. Wolski, P. Dhariwal, A. Radford, and O. Klimov, "Proximal policy optimization algorithms," *arXiv preprint arXiv:1707.06347*, 2017.
- [27] P. Dhariwal, C. Hesse, O. Klimov, A. Nichol, M. Plappert, A. Radford, J. Schulman, S. Sidor, Y. Wu, and P. Zhokhov, "Openai baselines," <https://github.com/openai/baselines>, 2017.
- [28] P. Warden, "Speech commands: A dataset for limited-vocabulary speech recognition," *arXiv preprint arXiv:1804.03209*, 2018.
- [29] J. Engel, C. Resnick, A. Roberts, S. Dieleman, D. Eck, K. Simonyan, and M. Norouzi, "Neural audio synthesis of musical notes with wavenet autoencoders," in *International Conference on Machine Learning (ICML)*, 2017, pp. 1068–1077.
- [30] J. Lyons, "Python speech features," <https://github.com/jameslyons/python-speech-features>, 2013–2019.
- [31] E. Coumans and Y. Bai, "Pybullet, a python module for physics simulation for games, robotics and machine learning," <http://pybullet.org>, 2016–2019.
- [32] J. Tobin, R. Fong, A. Ray, J. Schneider, W. Zaremba, and P. Abbeel, "Domain randomization for transferring deep neural networks from simulation to the real world," *IEEE/RSJ International Conference on Intelligent Robots and Systems (IROS)*, pp. 23–30, 2017.
- [33] M. Cimpoi, S. Maji, I. Kokkinos, S. Mohamed, and A. Vedaldi, "Describing textures in the wild," in *IEEE Computer Society Conference on Computer Vision and Pattern Recognition (CVPR)*, 2014.
- [34] M. Quigley, K. Conley, B. Gerkey, J. Faust, T. Foote, J. Leibs, R. Wheeler, and A. Y. Ng, "Ros: an open-source robot operating system," in *IEEE International Conference on Robotics and Automation (ICRA) Workshop on Open Source Software*, vol. 3, no. 3.2, 2009, p. 5.
- [35] "ROS Packages for TurtleBot3 by ROBOTIS," https://github.com/ROBOTIS-GIT/turtlebot3/tree/master/turtlebot3_navigation, 2019.